The impact of chaotic saddles on the synchronization of complex networks of discrete-time units

View the article online for updates and enhancements.

Journal of Physics: Complexity

The impact of chaotic saddles on the synchronization of complex networks of discrete-time units

Everton S Medeiros[1],[*] , Rene O Medrano-T[2],[3], Iberê L Caldas[4] and Ulrike Feudel[5]

1   Institut für Theoretische Physik, Technische Universität Berlin, Hardenbergstraße 36, 10623 Berlin, Germany
2   Departamento de Física, Universidade Federal de São Paulo, Campus Diadema, R. São Nicolau, 210, 09913-030 SP, Brazil
3   Departamento de Física, Universidade Estadual Paulista, Instituto de Geociências e Ciências Exatas, Campus Rio Claro, Av. 24A, 1515, 13506-900 SP, Brazil
4   Institute of Physics, University of São Paulo, Rua do Matão, Travessa R 187, 05508-090, São Paulo, Brazil
5   Institute for Chemistry and Biology of the Marine Environment, Carl von Ossietzky University of Oldenburg, Oldenburg, Germany
*   Author to whom any correspondence should be addressed.

E-mail: medeiros@tu-berlin.de

Abstract

A chaotic saddle is a common nonattracting chaotic set well known for generating finite-time chaotic behavior in low and high-dimensional systems. In general, dynamical systems possessing chaotic saddles in their state-space exhibit irregular behavior with duration lengths following an exponential distribution. However, when these systems are coupled into networks the chaotic saddle plays a role in the long-term dynamics by trapping network trajectories for times that are indefinitely long. This process transforms the network's high-dimensional state-space by creating an alternative persistent desynchronized state coexisting with the completely synchronized one. Such coexistence threatens the synchronized state with vulnerability to external perturbations. We demonstrate the onset of this phenomenon in complex networks of discrete-time units in which the synchronization manifold is perturbed either in the initial instant of time or in arbitrary states of its asymptotic dynamics. The role of topological asymmetries of Erdös–Rényi and Barabási–Albert graphs are investigated. Besides, the required coupling strength for the occurrence of trapping in the chaotic saddle is unveiled.

1. Introduction

Chaotic saddles are ubiquitous across dynamical systems. Such non-attracting chaotic sets appear in the system's state-space caused by a variety of mechanisms. For instance, they emerge as a result of a boundary crisis [1, 2], in which a chaotic attractor loses stability [3]. They also appear via a basin boundary metamorphosis [4], in which a smooth boundary turns into a fractal, or even, via an embedded saddle-node bifurcation at which the basin boundary of a stable fixed point collides with the chaotic attractor converting it into a chaotic saddle [5, 7]. This mechanism can be observed when a periodic window within a chaotic parameter range is created—a situation relevant for the study here. Moreover, there are other mechanisms for the appearance of such nonattracting chaotic sets, e.g., outer homoclinic and heteroclinic tangencies [6, 7]. Chaotic saddles play an essential role in the dynamics of various applications, such as e.g. in chaotic scattering processes [8–10]; in spatially extended dynamical systems [11, 12]; in the hopping dynamics between different coexisting attractors in a multistable system [13]; in controlling long chaotic transients [14]; in the control of dynamical systems either to sustain chaos [15] or to drive the system toward desired attractors [16] or terminating chaotic transients [17]. In complex networks of oscillators chaotic saddles can be responsible for the switching between different space–time patterns [18]. Chaotic saddles are also of great importance in hydrodynamics. There, the signatures of chaotic saddles can be detected via the fractal boundaries in open hydrodynamical flows [19]. In the transition to turbulence in a pipe flow, the chaotic saddle acts as a threshold separating the laminar flow from turbulent intermittency, often called the edge of chaos [20, 21]. In chaotic advection, the fractal structure of chaotic saddles is responsible for the enhancement of particle concentrations [22], and also for

trapping aerosols in their neighborhood preventing escaping in open flows [23]. In noisy dynamics, chaotic saddles constitute the backbone of long-living erratic trajectories in a phenomenon called noise-induced chaos [24]. Finally, one of the most known features of chaotic saddles is the generation of finite-time chaotic behavior in deterministic dynamical systems ranging from simple discrete-time maps to partial differential equations [25, 26].

In networked dynamical systems, chaotic saddles may be present in the state-space of individual system units. In this scenario, the attractive character of the network coupling creates a synchronization manifold, i.e., all units behave identically in time. Normally, such an invariant manifold would oscillate chaotically in the vicinity of the underlying chaotic saddle before converging to its asymptotic dynamics in times exponentially distributed. However, under the effect of external perturbations, the synchronization manifold may break down and, consequently, the network units go across the chaotic saddle with individual trajectories. This mechanism gives rise to an interaction between the chaotic dynamics in the saddle and the network coupling strength. Such interplay postpones the permanency of units in the chaotic saddle for times that are indefinitely long, suppressing the occurrence of synchronization in the network [27, 28]. Therefore, the occurrence of this kind of vulnerability affects many systems relying on synchronization to function properly. Yet, the role of asymmetrical network topologies such as the ones with nontrivial degree distribution is still unclear.

In this work, we examine the vulnerability of synchronized states in networks possessing chaotic saddles in the state-space of their units. Our networks are composed of identical Hénon maps coupled via complex topologies such as Erdös–Rényi (ER) and Barabási–Albert (BA) graphs. First, we study the vulnerability of the synchronization manifold to perturbations occurring at the initial time instant. This vulnerability is demonstrated by attributing a different initial condition (IC) to one of the network units (perturbed unit), while the remaining units receive identical values. By investigating the occurrence of complete synchronization in the network for different ICs attributed to the perturbed unit, we verify that the occurrence of completely synchronized states is sensitively dependent on the choice of ICs. In addition, we observe that the relative portion of ICs attributed to perturbed units leading to synchronized states is significantly lower for perturbing units with a high degree. These results are demonstrated by computing the single-node basin stability as a function of the unit's degree in a Barabási–Albert graph.

Next, we investigate the state-dependent vulnerability, i.e., perturbations are applied directly to asymptotic dynamical states visited by the synchronization manifold. By performing a comprehensive analysis of the perturbation amplitudes, we find that the perturbation sets leading the network to desynchronization are intermingled with the ones at which synchronization is restored. In addition, we verify that the vulnerability of the synchronization manifold also depends on the dynamical state at which the perturbation is applied. This dependence is demonstrated by assessing the effects of a given perturbation in consecutive states of the synchronization manifold trajectory. Finally, we investigate the intervals of the network coupling strength for which the interaction with the chaotic saddle generates vulnerabilities.
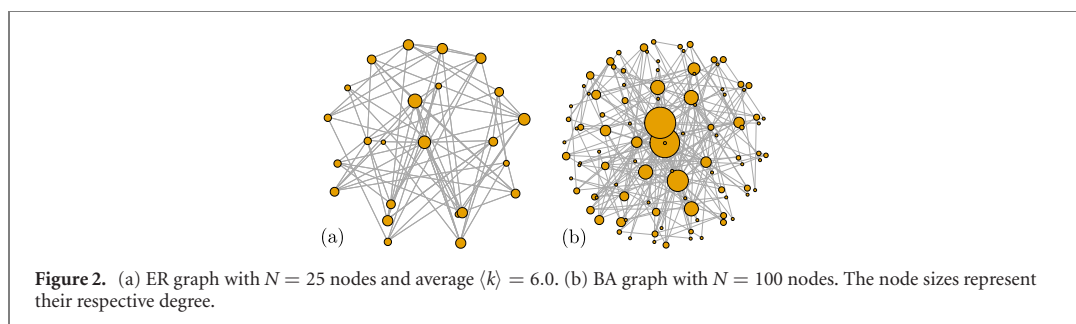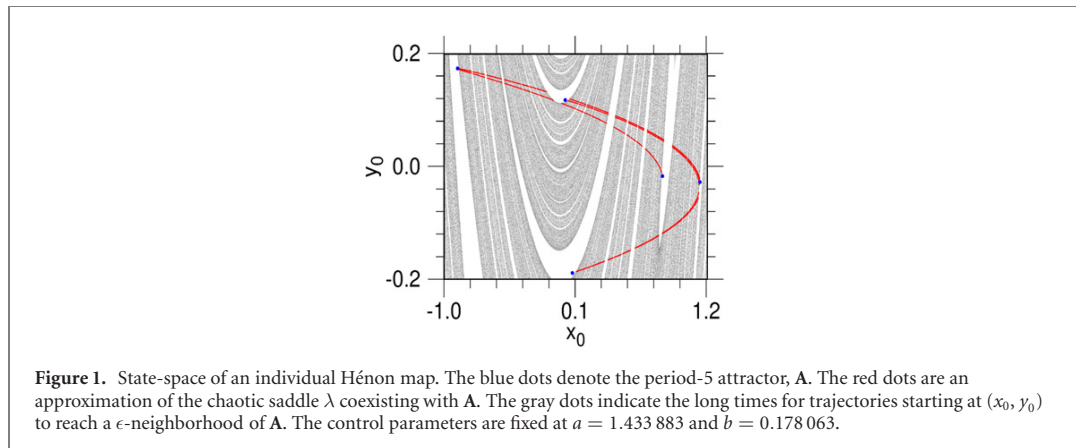
2. System dynamics

To illustrate the impact of chaotic saddles on the long-term dynamics of networked discrete-time systems, we consider an ER graph with Hénon maps oscillating in its nodes. The high-dimensional equations describing this system are given by:

$$x_i^{t+1} = f(x_i^t, y_i^t) + \frac{\sigma}{D_i} \sum_{j \in \mathcal{D}_i} [f(x_j^t, y_j^t) - f(x_i^t, y_i^t)],$$

$$y_i^{t+1} = g(x_i^t, y_i^t) + \frac{\sigma}{D_i} \sum_{j \in \mathcal{D}_i} [g(x_j^t, y_j^t) - g(x_i^t, y_i^t)], \tag{1}$$

where the functions $f(x, y) = 1 - ax^2 + y$ and $g(x, y) = bx$ provide the dynamics of the Hénon maps in the network. The parameter set (a, b) specifies the dynamical behavior of each individual map. In this study, we fix these parameters at $a = 1.433\,883$ and $b = 0.178\,063$, whereas after a chaotic transient, the isolated maps oscillate in a period-5 attractor **A** denoted by the blue dots in figure 1. The vector $\mathbf{v}_i^t = (x_i^t, y_i^t)$ defines the state space of each Hénon unit i in the network with $i = 1, \dots, N$. The constant σ controls the coupling strength among the units. Following the ER graph shown in figure 2(a), $\mathcal{D}_i$ specifies the set of network units adjacent to a given unit i, while the parameter D_i is the number of units to which the node i is connected.

First, by considering $\sigma = 0$ in equation (1), we investigate the individual dynamics of the Hénon maps composing the network. Besides the aforementioned period-5 attractor, **A**, an unstable chaotic set λ (chaotic saddle) occurs in the system's state-space. In figure 1, we show in red an approximation of the chaotic saddle λ, obtained via the sprinkler method [26]. The gray dots are an approximation of the stable manifold of this

Figure 1. State-space of an individual Hénon map. The blue dots denote the period-5 attractor, **A**. The red dots are an approximation of the chaotic saddle λ coexisting with **A**. The gray dots indicate the long times for trajectories starting at (x_0, y_0) to reach a ϵ-neighborhood of **A**. The control parameters are fixed at $a = 1.433\,883$ and $b = 0.178\,063$.

Figure 2. (a) ER graph with $N = 25$ nodes and average $\langle k \rangle = 6.0$. (b) BA graph with $N = 100$ nodes. The node sizes represent their respective degree.

saddle obtained via the long time for trajectories to reach a ϵ-neighborhood of the attractor ($\epsilon = 10^{-3}$). The 5 blue dots indicate the period-5 attractor.

At the level of the units, all trajectories starting in the (x_0, y_0)-interval shown in figure 1 will ultimately converge to the period-5 attractor. However, the ICs signaled in gray in this figure will first approach the chaotic saddle, oscillate chaotically in its neighborhood, and finally will escape toward the attractor. This state-space characteristics of each individual Hénon map will play an essential role in the dynamics of the coupled system.

3. Vulnerability with respect to the initial state

Recently, for a symmetrically coupled network of Duffing oscillators, the chaotic saddle has been found to play a decisive role in the final state sensitivity of the network [27]. Specifically, the convergence to a completely synchronized state or a desynchronized one depends sensitively on the system's ICs. This is due to a nontrivial interaction between the chaotic saddle and the network coupling, which in reference [27] is symmetric. Here, we investigate the effects of the saddle–coupling interaction in the presence of network asymmetries such as the ones in ER and BA graphs shown in figures 2(a) and (b), respectively. An ER graph, also called random graph, consists of N nodes connected by L randomly distributed links. Due to the random character of the link assignments, the number of links varies among the nodes. Specifically, the number of links of a given node, i.e., the node degree k, follows a Poisson distribution with average value $\langle k \rangle$. Conversely, in the construction of a BA graph, also called scale-free network, the concept of preferential attachment is incorporated resulting in a growth algorithm where new nodes are more likely to be attached to more connected nodes. This procedure results in large variabilities in the number of connections among the nodes, with the presence of highly connected nodes, so-called hubs, absent in random graphs. Based on this construction, BA graphs possess a power-law distribution of degrees as a stationary scale-free state, i.e., the power-law correlation is independent of the graph size and growth time. For the purpose of our investigations, both ER and BA graphs provide the required topological asymmetries. Nonetheless, in figure 5, we assess their vulnerability to the effects of the chaotic saddle. For the network described by equation (1), the synchronized state of the high-dimensional system lies in a synchronization manifold **S**, defined as $\mathbf{v}_1^t = \mathbf{v}_2^t = \cdots = \mathbf{v}_N^t$. We denote the states visited by the synchronization manifold **S** in the period-5 orbit as $\mathbf{v}_S^t = (x_S^t, y_S^t)$.

In order to quantify the influence of the chaotic saddle λ on the global dynamics of the network, we perturb the synchronization manifold **S** in the initial instant of time ($t = 0$), i.e., in the initial state $\mathbf{v}_S^0 = (x_S^0, y_S^0)$.
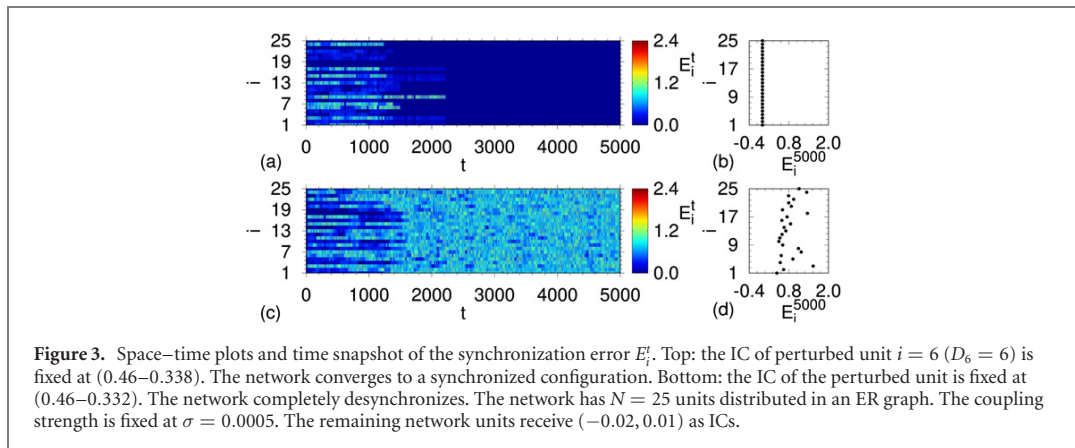
Figure 3. Space−time plots and time snapshot of the synchronization error E_i^t. Top: the IC of perturbed unit $i = 6$ ($D_6 = 6$) is fixed at (0.46−0.338). The network converges to a synchronized configuration. Bottom: the IC of the perturbed unit is fixed at (0.46−0.332). The network completely desynchronizes. The network has $N = 25$ units distributed in an ER graph. The coupling strength is fixed at $\sigma = 0.0005$. The remaining network units receive $(-0.02, 0.01)$ as ICs.

This strategy is realized by defining the ICs of the units at a common value $\mathbf{v}_i^0 = (-0.02, 0.01)$ except for one unit chosen to be the perturbation to **S**. For instance, in the space−time plot shown in figure 3(a), the unit $i = 6$ with degree $D_6 = 6$ acts as a perturbation to **S** by receiving the IC $\mathbf{v}_6^0 = (0.460, -0.338)$. The color code indicates the local synchronization error defined as $E_i^t = 1/D_i \sum_{j \in \mathcal{D}_i} \|\mathbf{v}_i^t - \mathbf{v}_j^t\|$ with $i = 1, \ldots, N$. With this, we observe that after an initial phase of desynchronized behavior in a large portion of the network, all units approach **S** following the period-5 attractor. In figure 3(b), we show a spatial snapshot of the synchronization error, E_i^{5000}. In figure 3(c), we attribute a slightly different IC to the same unit $i = 6$, this time, $\mathbf{v}_6^0 = (0.460, -0.332)$. Differently from the previous scenario, the network goes toward a state of complete desynchronization. The spatial snapshot at $t = 5000$ time steps shown in figure 3(d) confirms the desynchronized behavior. Hence, such sensitivity to the ICs observed in figure 3 indicates that the chaotic saddle presents in every unit in the uncoupled case influences the global dynamics of the network.
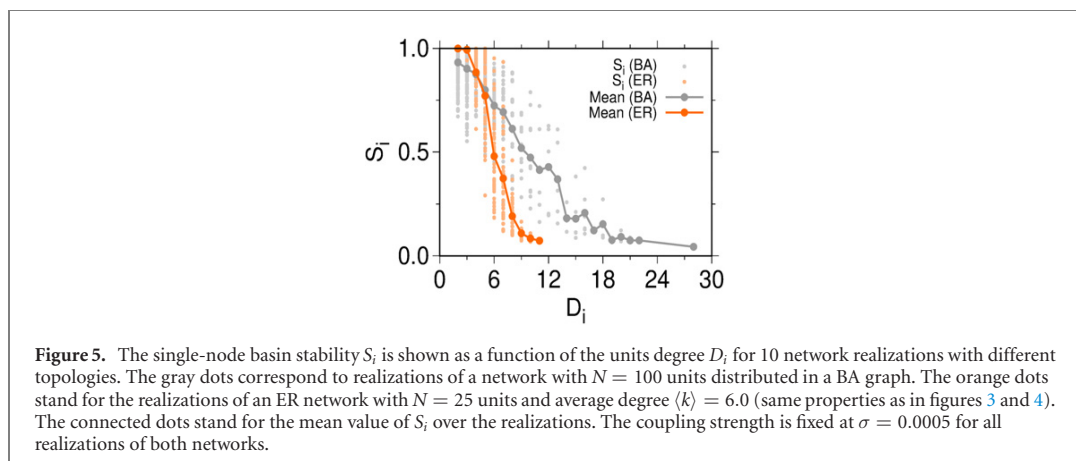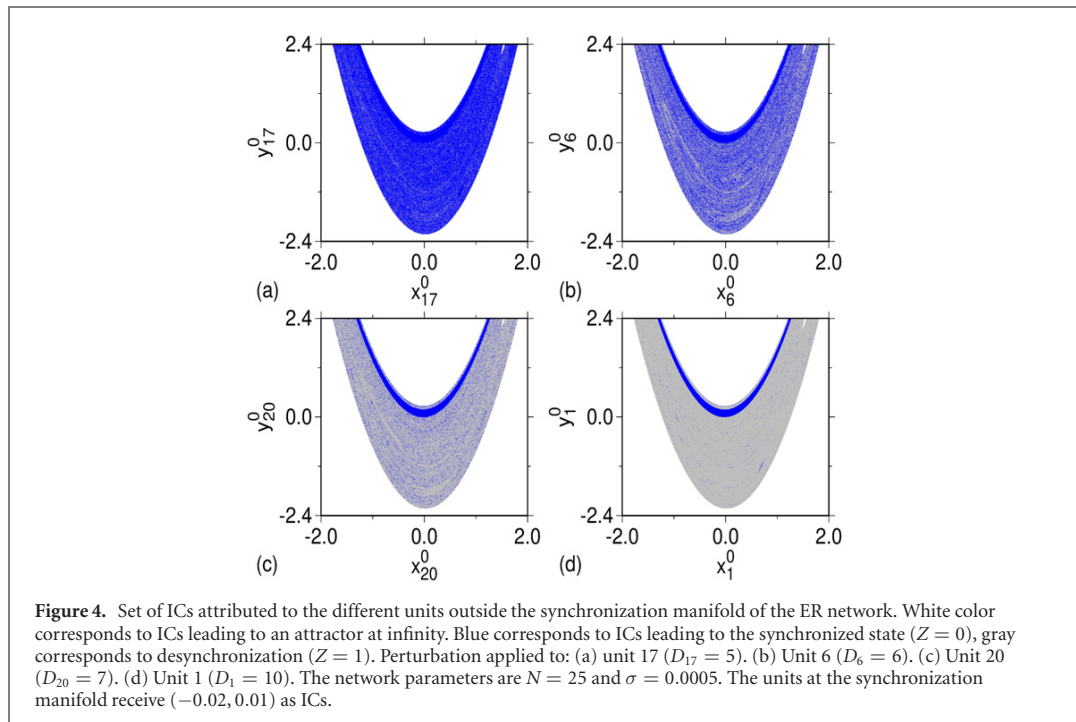
Given the topological asymmetries of the ER graph specifying the network structure in equation (1), we ask the question of how synchronization would be affected by perturbing units with different degrees, D_i. Before addressing this issue, we define a measure to assess the levels of synchronization in the entire network. With this, by analyzing the local synchronization error E_i^t, we define the global synchronization error $\mathcal{Z}$ as:

$$\mathcal{Z} = \frac{1}{N} \sum_{i=1}^{N} K_i, \quad K_i = \begin{cases} 1, & \text{if } E_i^{t_f} > \delta \\ 0, & \text{if } E_i^{t_f} < \delta. \end{cases} \tag{2}$$

The parameter δ establishes the synchronization quality ($\delta = 0.01$) and t_f is the overall number of iterations of the network ($t_f = 5 \times 10^4$ steps). Hence, the completely synchronized state returns a global synchronization error $\mathcal{Z} = 0$, while the completely desynchronized state implies a global synchronization error $\mathcal{Z} = 1$.
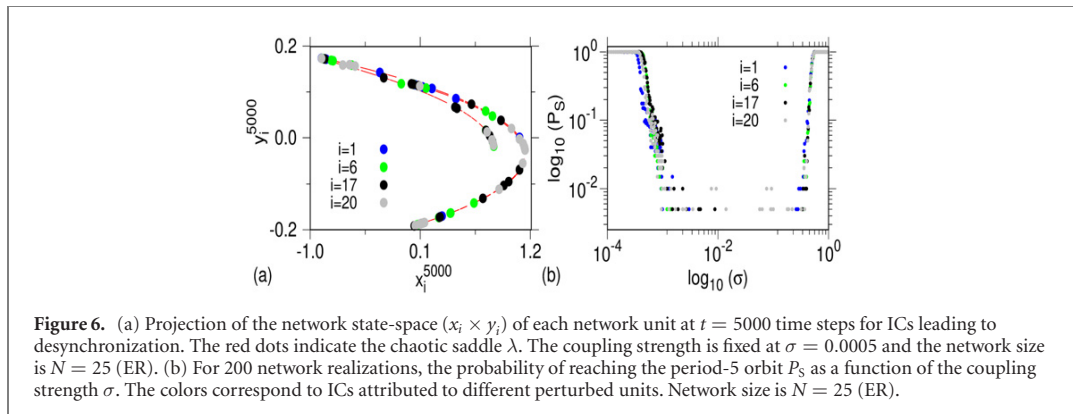
Now, in figure 4, we compute $\mathcal{Z}$ for two-dimensional intervals of ICs attributed to perturbed units. In this figure, the dots marked in blue corresponds to ICs leading to synchronization ($\mathcal{Z} = 0$), while the ones marked in gray indicate ICs leading the entire network to a desynchronized configuration ($\mathcal{Z} = 1$). These diagrams constitute two-dimensional sections of the system's $2N$-dimensional basin of attraction. First, in figure 4(a), we show the interval of ICs attributed to the unit $i = 17$, specifically, $x_{17}^0 \in [-2.0, 2.0]$ and $y_{17}^0 \in [-2.4, 2.4]$. This unit has a relatively low degree, $D_{17} = 5$. For this case, we observe that the ICs leading the network to synchronized behavior, the sync basin (blue dots), are predominant. Nevertheless, the sparse ICs corresponding to desynchronized behavior in the network appears intermingled with the sync basin. Next, in figure 4(b), we consider the same interval of ICs but perturb the unit $i = 6$ with $D_6 = 6$. In this case, the sync basin is already smaller than in the previous scenario giving rise to more ICs leading to desynchronized behavior. In the interest of further increase of the degree of the perturbed units, in figure 4(c), we show the effects of perturbing the unit $i = 20$ with $D_{20} = 7$. The fraction of ICs leading the network to desynchronization is now larger than the ones leading to synchronized behavior. The intermingled aspect of the basins is still visible even though areas with a higher density of desynchronizing ICs appear. Finally, in figure 4(d), we show the basin of attraction in the cross-section (x_i, y_i) of the unit $i = 1$ with $D_1 = 10$. In this case, the ICs leading to desynchronized behavior dominate the picture leaving only a small number of ICs for the sync basin.

The results shown in figure 4 illustrate that the network is highly sensitive to the choice of the ICs attributed to the perturbed unit regardless of the degree of connections of such a unit. However, the relative volume of the basin of attraction leading to synchronization, computed as the number of ICs in the sync basin divided by the total number of ICs, is lower for perturbed units possessing a higher degree, see figures 4(a) and (d).

Figure 4. Set of ICs attributed to the different units outside the synchronization manifold of the ER network. White color corresponds to ICs leading to an attractor at infinity. Blue corresponds to ICs leading to the synchronized state ($Z = 0$), gray corresponds to desynchronization ($Z = 1$). Perturbation applied to: (a) unit 17 ($D_{17} = 5$). (b) Unit 6 ($D_6 = 6$). (c) Unit 20 ($D_{20} = 7$). (d) Unit 1 ($D_1 = 10$). The network parameters are $N = 25$ and $\sigma = 0.0005$. The units at the synchronization manifold receive $(-0.02, 0.01)$ as ICs.

Figure 5. The single-node basin stability S_i is shown as a function of the units degree D_i for 10 network realizations with different topologies. The gray dots correspond to realizations of a network with $N = 100$ units distributed in a BA graph. The orange dots stand for the realizations of an ER network with $N = 25$ units and average degree $\langle k \rangle = 6.0$ (same properties as in figures 3 and 4). The connected dots stand for the mean value of S_i over the realizations. The coupling strength is fixed at $\sigma = 0.0005$ for all realizations of both networks.

To further elucidate this dependence, we look at ensembles of network realizations with different topologies. First, we generate 10 different ER graphs of the same size and average degree as addressed in figure 4, i.e. $N = 25$ and $\langle k \rangle = 6.0$. In addition, we consider 10 realizations of networks with $N = 100$ units arranged in BA graphs possessing a power-law degree distribution [29], see figure 2(b). Next, we investigate the effect of perturbing units with different degrees for the ensembles of the two network categories. For this, we estimate the relative volume of the basin of attraction of the synchronized state for different units using the concept of *basin stability* [30]. Here, similarly to reference [31], basin stability is computed for single-nodes, i.e. in a two-dimensional cross-section of the $2N$-dimensional state-space. For every unit i, we consider a finite portion of the cross-section (x_i^0, y_i^0), namely, $x_i^0 \in [-2.0, 2.0]$ and $y_i^0 \in [-2.4, 2.4]$. Hence, in figure 5, we show the single-node basin stability S_i obtained for every unit i as a function of its degree D_i in both proposed graphs categories for every network realization as well as the averaged S_i over the ensembles.

From figure 5, one can conclude that the relative volume of the unit's state-space leading the network to synchronization becomes significantly lower with the increasing degree for both, the ER and the BA networks. Therefore, the trapping of trajectories in the chaotic saddle as a consequence of the interaction between network units due to their coupling is much more prominent for perturbing units with a higher degree. These results confirm the evidence raised in figures 4(a)–(d) for only one realization of an ER network. Besides, in figure 5, for most of the investigated degree interval, we observe that the averaged single-node basin stability

Figure 6. (a) Projection of the network state-space ($x_i \times y_i$) of each network unit at $t = 5000$ time steps for ICs leading to desynchronization. The red dots indicate the chaotic saddle λ. The coupling strength is fixed at $\sigma = 0.0005$ and the network size is $N = 25$ (ER). (b) For 200 network realizations, the probability of reaching the period-5 orbit P_S as a function of the coupling strength σ. The colors correspond to ICs attributed to different perturbed units. Network size is $N = 25$ (ER).

is lower for ER networks compared to units on BA networks with the same degree. This suggests that the ER networks are more susceptible to the effects of the chaotic saddle. However, the general characteristics of the investigated network topologies such as their size and their average degree play an essential role in the global stability of the synchronized state. Since the impact of these aspects is beyond the scope of this study, any conclusion on which network category is most influenced by the chaotic saddle is left open for future investigations aiming at a comprehensive view on the consequences of the topological characteristics.

The similarities between the basin of the desynchronized state in figure 4 and the approximation of stable manifold of the chaotic saddle shown in figure 1 suggest a close relationship between them. To emphasize this relationship, we show snapshots of the network trajectories at the time $t = 5000$ times steps (figure 6(a)). The large dots represent the network units ($N = 25$), the colors correspond to a snapshot of trajectories originating from different perturbed units. Indeed, we verify that the interaction between the chaotic dynamics in the saddle and the network coupling traps the network trajectory in the vicinity of the saddle (red dots in figure 6(a)). This phenomenon occurs for a limited range of the network coupling strength σ as shown in figure 6(b). In this figure, we consider $n = 200$ realizations of the ER network with different ICs attributed to a given perturbed unit ($i = 1$, $i = 6$, $i = 17$, or $i = 20$). From this ensemble, we compute the probability $P_S = n_S/n$, where n_S corresponds to realizations in which all units are close to the period-5 attractor **A**, i.e. escape from the chaotic saddle. Hence, in figure 6(b) we show P_S as function of σ and for different perturbed units exhibiting different degrees (color code).

The results shown in figure 6(b) illustrate that the occurrence of the network trapping in the chaotic saddle depends strongly on the choice of σ rather than the degree of the perturbed unit. We also point out that this phenomenon is very robust since it occurs for many orders of magnitude of the coupling strength σ. Only for very strong coupling strength, the synchronized state is globally stable. Please note, that for intermediate coupling strength not a single out of 200 realizations leads to synchronization.

The mechanism at which the synchronized period-5 solution exhibits the aforementioned intricate dependence on the perturbation applied to an arbitrarily chosen unit lies in the interplay between the chaotic saddle and the coupling between the units. When one unit is perturbed by a specific vector, its state variables will be placed in another point of the state space. In the case that this point is close to the stable manifold of the chaotic saddle, the trajectory of the perturbed unit will approach the chaotic saddle along its stable manifold. Since the perturbed unit is coupled to other units, it will pull additional units also in a direction to leave the synchronization manifold toward the chaotic saddle. At this point, the interplay between the chaotic saddle and the coupling can then lead the network to a complete desynchronized state. By contrast, when the perturbation vector is slightly different, the state variables of the perturbed unit will end up at a different point in state space which might not be close enough to the saddle's stable manifold. In that case, the network coupling can restore the synchronized state. Since the stable manifolds of the chaotic saddle have a very intricate structure in the system state-space, points close to it and points far from it are complexly interwoven. Consequently, the synchronized solution is highly sensitive to perturbations at the initial instant of time. In summary, the motion of the perturbed unit close to the chaotic saddle initially desynchronizes a subset of the network units by bringing it also close to the chaotic saddle. The longer the trajectories of that subset stay in the chaotic regime, the larger gets the likelihood of additional units joining this subset via the action of the coupling. In turn, as the subset of desynchronized units grows, the mutual disturbances among its units give rise to an even lower likelihood of escaping the saddle's neighborhood. As a consequence, after a critical number of units oscillate close to the chaotic saddle, the state of complete desynchronization becomes accessible. This mechanism is discussed in detail in reference [27] for a symmetric network of continuous-time units.
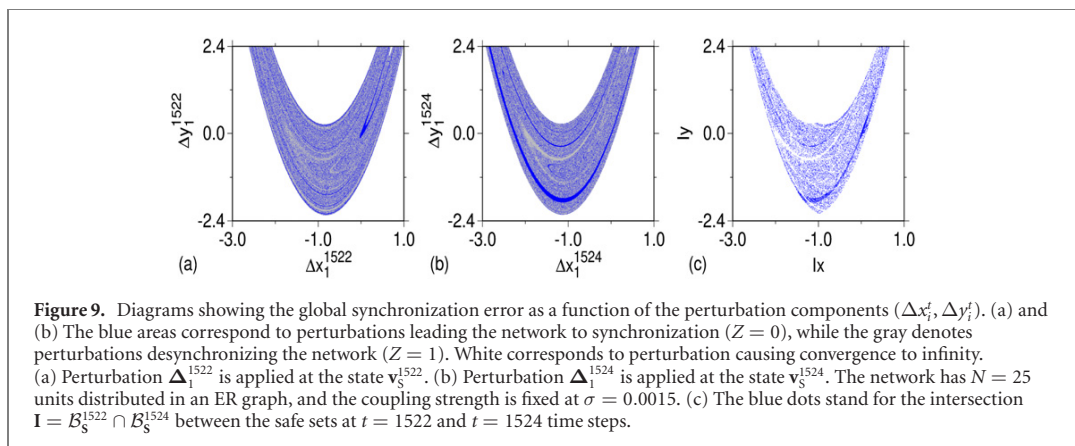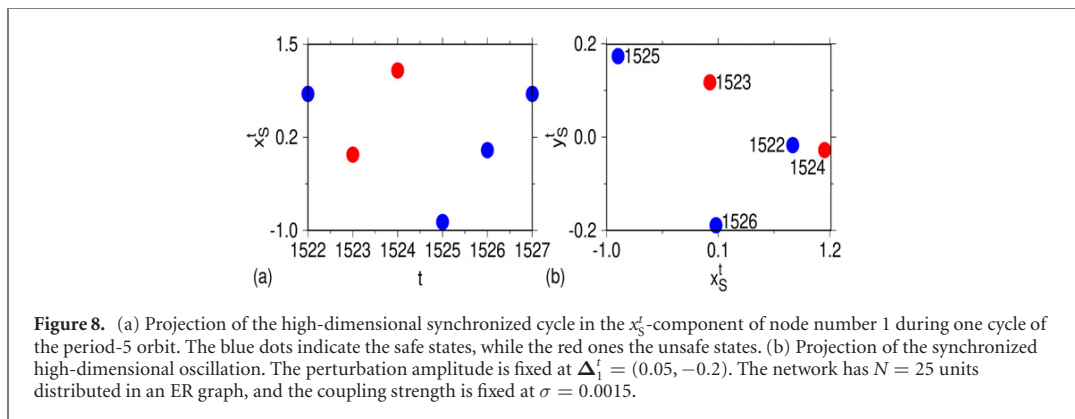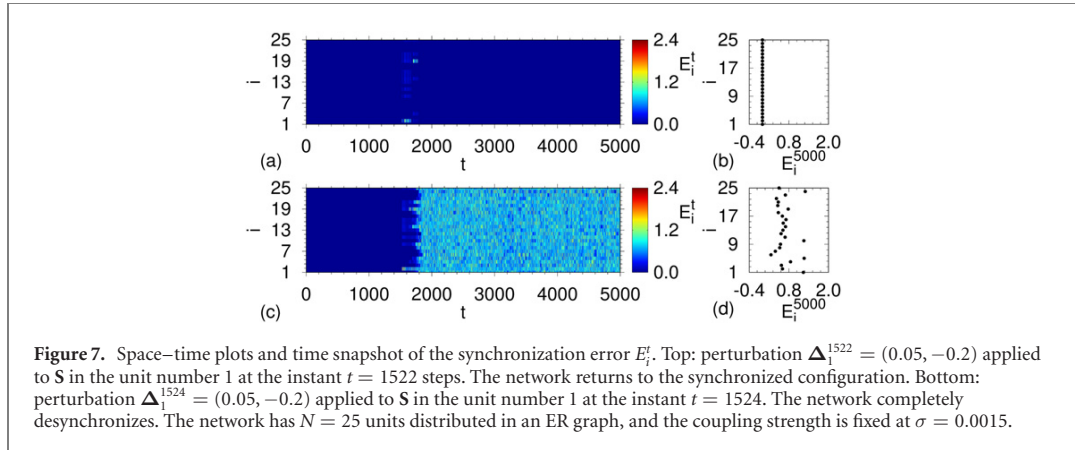
4. State-dependent vulnerability

Remarkably, the presence of the chaotic saddle λ in the state-space of the discrete-time units composing the network described in equation (1) has consequences not only for perturbations at $t = 0$. In fact, even after the whole network is completely synchronized in the period-5 attractor, perturbations in the different states of this solution may still desynchronize the system. Similar state-dependent phenomena have been recently reported in the vulnerability of synchronization in a network of continuous-time units [28], in the excitability of a limit-cycle [32], and in the survivability of the solitary states in a multiplex network [33].

To demonstrate this state-dependent vulnerability in an ER network of discrete-time units, we first consider the space–time diagrams of figure 7. In these diagrams, all units are initialized such that they reach the period-5 attractor. Hence, the synchronization manifold follows the trajectory specified by $\mathbf{v}_S^t = (x_S^t, y_S^t)$. Specifically, we define the synchronization manifold **S** at $t = 0$ by attributing the IC $(0.3, 0.2)$ to all network units. After transients, when the system reaches the attractor, we apply an external perturbation at any of the five states $\mathbf{v}_S^t$ belonging to the attractor of the synchronized high-dimensional system. The perturbation is defined as a deviation $\boldsymbol{\Delta}_i^t = (\Delta x_i^t, \Delta y_i^t)$ and applied directly to the dynamics of a specific unit i exactly in that moment when this is at the state $\mathbf{v}_S^t$. This is illustrated in figure 7(a), where we apply the perturbation $\boldsymbol{\Delta}_1^{1522} = (0.05, -0.2)$ at the state $\mathbf{v}_S^{1522}$ corresponding to the iteration at $t = 1522$ time steps and the unit $i = 1$. The color code in the figure indicates the synchronization error $E_i^t = 1/D_i \sum_{j \in \mathcal{D}_i} \|\mathbf{v}_i^t - \mathbf{v}_j^t\|$ with $i = 1, \ldots, N$. We observe that after a very small time interval with desynchronized behavior right after $t = 1522$ time steps the system returns to the synchronized configuration. This result is emphasized by the snapshot of the dynamics of the whole network at $t = 5000$ time steps showing $E_i^t = 0$ in figure 7(b). Now, we apply the same perturbation $\boldsymbol{\Delta}_1^{1524} = (0.05, -0.2)$ at the same unit $i = 1$ but at a different state of the period-5 attractor, namely at the time $t = 1524$ steps. As an outcome, in figure 7(c), we observe the entire network approaching a completely desynchronized behavior. This observation is supported by the snapshot at $t = 5000$ time steps shown in figure 7(d).

The sensitivity observed in figure 7 suggests a state-dependent vulnerability of the synchronized state. To clarify this behavior, we show in figure 8(a) each of the x_S^t-components during one cycle of the synchronized period-5 orbit using a color code indicating the state-dependent vulnerability to the perturbation $\boldsymbol{\Delta}_1^t = (0.05, -0.2)$. In blue are the states at which the system returns to synchronization after $\boldsymbol{\Delta}_1^t$ is applied, the safe sets. The red points indicate the states $\mathbf{v}_S^{1523}$ and $\mathbf{v}_S^{1524}$ at which the same perturbation $\boldsymbol{\Delta}_1^t$ leads the whole network to desynchronization. These make up the unsafe set. In figure 8(b), we show a projection of the synchronized high-dimensional state space, (x_S^t, y_S^t) onto the two-dimensional state space of unit $i = 1$ oscillating in the period-5 orbit, the red dots show the region occupied by the unsafe set. In both figures 8(a) and (b), the synchronization is assessed by the global synchronization error $\mathcal{Z}$ defined in equation (2).
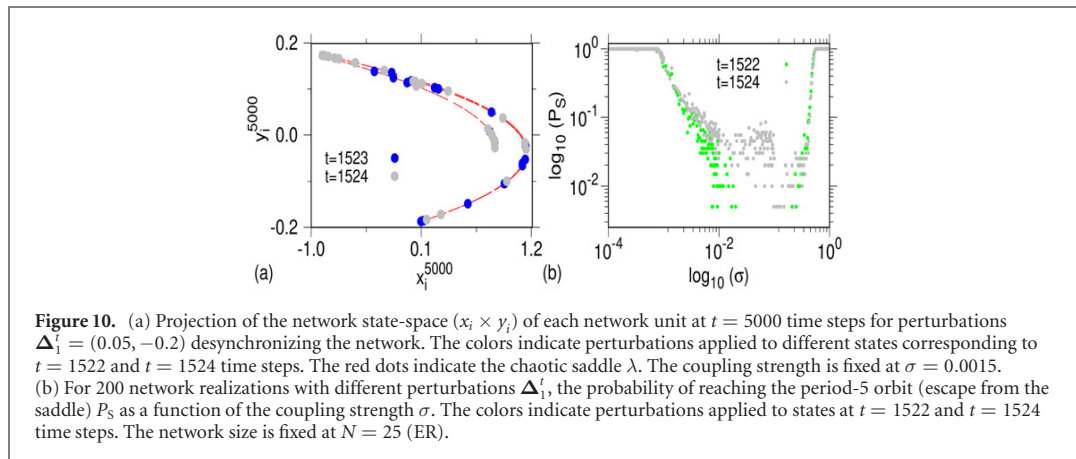
To shed more light on the role of the amplitude of the perturbations $\boldsymbol{\Delta}_i^t$ played in such state-dependent vulnerability, we investigate the sets of perturbations in x–y state where $(\Delta x_i^t, \Delta y_i^t)$ stands for the amplitude of each component of the perturbation. In figure 9(a), we obtain such a diagram for the perturbation $\boldsymbol{\Delta}_1^{1522}$. The color code denotes the global synchronization error Z. Specifically, blue color indicates perturbation regions for which the network synchronizes ($Z = 0$) after the perturbation ($t = 1522$ time steps), the safe set denoted by $\mathcal{B}_S^{1522}$. The gray color indicates regions for which the perturbation at $t = 1522$ time steps leads the entire network to desynchronization ($Z = 1$), the unsafe set denoted by $\mathcal{B}_\lambda^{1522}$. Regions in white indicate perturbations for which the solution converges to the attractor at infinity. In figure 9(b), we obtain the same diagram for the perturbation applied in a different state, at $t = 1524$ time steps. Despite visual similarities between the diagram obtained for both states, internally, the structures are significantly different. This indicates that a whole set of perturbations that are safe when applied in a given state have a different outcome in another state. We illustrate this phenomenon in figure 9(c) by estimating the intersection $\mathbf{I} = \mathcal{B}_S^{1522} \cap \mathcal{B}_S^{1524}$ between the safe sets obtained for $t = 1522$ and $t = 1524$ time steps.

Similar to the initial-state vulnerability discussed in section 3, the trajectories of the desynchronized network are trapped in the neighborhood of the chaotic saddle λ. We demonstrate this result in figure 10(a) for the perturbation $\boldsymbol{\Delta}_1^t = (0.05, -0.2)$ applied in the dynamical states corresponding to the instants $t = 1523$ steps (blue dots) and $t = 1524$ steps (gray dots). The robustness of the trapping phenomenon with respect to changes in the coupling strength σ of the network is also assessed for the state-dependent vulnerability. For that, in figure 10(b), we consider $n = 200$ realizations of our network with different perturbation amplitudes $\boldsymbol{\Delta}_1^t$ applied in the instants $t = 1522$ steps (green dots) and $t = 1524$ steps (gray dots). By recording the realizations n_S in which all units are close to the period-5 attractor **A**, i.e. escape from the chaotic saddle, in figure 10(b), we show the probability $P_S = n_S/n$ as a function of coupling strength σ. Comparing these results with the ones for the perturbations at $t = 0$ shown in figure 6(b), we verify that for $t \neq 0$ the interval of σ with the occurrence of desynchronized behavior is slightly smaller. Additionally, in contrast to the IC vulnerability, the occurrence of solely desynchronized behavior, i.e., $P_S = 0$, does not occur at all.

Figure 7. Space–time plots and time snapshot of the synchronization error E_i^t. Top: perturbation $\mathbf{\Delta}_1^{1522} = (0.05, -0.2)$ applied to **S** in the unit number 1 at the instant $t = 1522$ steps. The network returns to the synchronized configuration. Bottom: perturbation $\mathbf{\Delta}_1^{1524} = (0.05, -0.2)$ applied to **S** in the unit number 1 at the instant $t = 1524$. The network completely desynchronizes. The network has $N = 25$ units distributed in an ER graph, and the coupling strength is fixed at $\sigma = 0.0015$.

Figure 8. (a) Projection of the high-dimensional synchronized cycle in the x_S^t-component of node number 1 during one cycle of the period-5 orbit. The blue dots indicate the safe states, while the red ones the unsafe states. (b) Projection of the synchronized high-dimensional oscillation. The perturbation amplitude is fixed at $\mathbf{\Delta}_1^t = (0.05, -0.2)$. The network has $N = 25$ units distributed in an ER graph, and the coupling strength is fixed at $\sigma = 0.0015$.

Figure 9. Diagrams showing the global synchronization error as a function of the perturbation components $(\Delta x_i^t, \Delta y_i^t)$. (a) and (b) The blue areas correspond to perturbations leading the network to synchronization ($Z = 0$), while the gray denotes perturbations desynchronizing the network ($Z = 1$). White corresponds to perturbation causing convergence to infinity. (a) Perturbation $\mathbf{\Delta}_1^{1522}$ is applied at the state $\mathbf{v}_S^{1522}$. (b) Perturbation $\mathbf{\Delta}_1^{1524}$ is applied at the state $\mathbf{v}_S^{1524}$. The network has $N = 25$ units distributed in an ER graph, and the coupling strength is fixed at $\sigma = 0.0015$. (c) The blue dots stand for the intersection $\mathbf{I} = \mathcal{B}_S^{1522} \cap \mathcal{B}_S^{1524}$ between the safe sets at $t = 1522$ and $t = 1524$ time steps.

The mechanism underlying the state-dependent vulnerability is the outcome of the interplay between the network coupling and the dynamics close to the chaotic saddle. A specific perturbation applied to the same units but at different time instants leads to different states of the network dynamics either close to the stable manifold of the chaotic saddle in one time instant and far away from it in the next time instant. As previously discussed in section 3, the trajectories which stay longer in the vicinity of the chaotic saddle increase the likelihood of having more network units approaching the saddle via pulling by the network coupling. After a critical number of units are following the chaotic saddle, in turn, the mutual disturbances decrease the likelihood of escaping and provide the grounds for a persistently long desynchronized solution [28].

In conclusion, we have demonstrated that chaotic saddles present in the dynamics of single discrete time units generate two distinct unpredictabilities to synchronized states in complex networks: (i) vulnerability of synchronization to localized perturbations applied at the initial state. For the network structure build in both

Figure 10. (a) Projection of the network state-space ($x_i \times y_i$) of each network unit at $t = 5000$ time steps for perturbations $\boldsymbol{\Delta}_1^t = (0.05, -0.2)$ desynchronizing the network. The colors indicate perturbations applied to different states corresponding to $t = 1522$ and $t = 1524$ time steps. The red dots indicate the chaotic saddle λ. The coupling strength is fixed at $\sigma = 0.0015$. (b) For 200 network realizations with different perturbations $\boldsymbol{\Delta}_1^t$, the probability of reaching the period-5 orbit (escape from the saddle) P_S as a function of the coupling strength σ. The colors indicate perturbations applied to states at $t = 1522$ and $t = 1524$ time steps. The network size is fixed at $N = 25$ (ER).

ER and BA graphs, the synchronization manifold is sensitively dependent on ICs attributed to specific network units. By computing the single-node basin stability for units with a power-law distribution of degrees (BA), we verify that perturbations applied to units with high degree (network hubs) reduce the relative size of the synchronization basin, therefore, are unsafe for synchronization. (ii) Vulnerability of synchronization to perturbation applied at arbitrary states of its asymptotic dynamics. For an ER topology, we verify that identical perturbations applied at different time instants, i.e. different states along the long-term trajectory produce different outcomes to synchronization. By inspecting large sets of perturbation amplitudes applied at two distinct states, we observe significant changes in the inner distribution of perturbations desynchronizing the network. For both vulnerability cases, we verify that the trajectories of the desynchronized network are indeed trapped in the vicinity of the chaotic saddle. Moreover, we unveil the regimes of the network coupling strength for the occurrence of this phenomenon. Finally, we remark that the trapping of trajectories in chaotic saddles may not be exclusive for networks of identical units. However, further details are open to future investigations.

Acknowledgments

Data availability statement

The data that support the findings of this study are available upon reasonable request from the authors.

ORCID iDs

Everton S Medeiros https://orcid.org/0000-0001-8531-6327

References

[1] Grebogi C, Ott E and Yorke J A 1982 *Phys. Rev. Lett.* **48** 1507
[2] Grebogi C, Ott E and Yorke J A 1983 *Physica* D **7** 181
[3] Ashwin P, Buescu J and Stewart I 1996 *Nonlinearity* **9** 703
[4] McDonald S W, Grebogi C, Ott E and Yorke J A 1985 *Phys. Lett.* A **107** 51
[5] Szabó K G, Lai Y-C, Tél T and Grebogi C 2000 *Phys. Rev.* E **61** 5019
[6] Robert C, Alligood K T, Ott E and Yorke J A 1998 *Phys. Rev. Lett.* **80** 4867
[7] Robert C, Alligood K T, Ott E and Yorke J A 2000 *Physica* D **144** 44

[8]   Ding M, Grebogi C, Ott E and Yorke J A 1990 *Phys. Rev. A* **42** 7025
[9]   Sweet D, Ott E and Yorke J A 1999 *Nature* **399** 315
[10] Aguirre J, Vallejo J C and Sanjuán M A 2001 *Phys. Rev. E* **64** 066208
[11] Lai Y-C and Winslow R L 1995 *Phys. Rev. Lett.* **74** 5208
[12] Rempel E L, Chian A C-L, Macau E E N and Rosa R R 2004 *Chaos* **14** 545
[13] Kraut S and Feudel U 2002 *Phys. Rev. E* **66** 015207
[14] Dhamala M and Lai Y-C 1999 *Phys. Rev. E* **59** 1646
[15] Schwartz I B and Triandaf I 1996 *Phys. Rev. Lett.* **77** 4740
[16] Macau E E N and Grebogi C 1999 *Phys. Rev. E* **59** 4062
[17] Lilienkamp T and Parlitz U 2020 *Chaos* **30** 051108
[18] Ansmann G, Lehnertz K and Feudel U 2016 *Phys. Rev. X* **6** 011030
[19] Péntek Á, Toroczkai Z, Tél T, Grebogi C and Yorke J A 1995 *Phys. Rev. E* **51** 4076
[20] Eckhardt B, Schneider T M, Hof B and Westerweel J 2007 *Annu. Rev. Fluid Mech.* **39** 447
[21] Schneider T M, Eckhardt B and Yorke J A 2007 *Phys. Rev. Lett.* **99** 034502
[22] Toroczkai Z, Károlyi G, Péntek Á, Tél T and Grebogi C 1998 *Phys. Rev. Lett.* **80** 500
[23] Vilela R D and Motter A E 2007 *Phys. Rev. Lett.* **99** 264101
[24] Tél T, Lai Y-C and Gruiz M 2008 *Int. J. Bifurcation Chaos* **18** 509
[25] Tél T and Lai Y-C 2008 *Phys. Rep.* **460** 245
[26] Lai Y-C and Tél T 2011 *Transient Chaos* (Berlin: Springer)
[27] Medeiros E S, Medrano-T R O, Caldas I L and Feudel U 2018 *Phys. Rev. E* **98** 030201
[28] Medeiros E S, Medrano-T R O, Caldas I L, Tél T and Feudel U 2019 *Phys. Rev. E* **100** 052201
[29] Barabási A-L and Albert R 1999 *Science* **286** 509
[30] Menck P J, Heitzig J, Marwan N and Kurths J 2013 *Nat. Phys.* **9** 89
[31] Mitra C, Choudhary A, Sinha S, Kurths J and Donner R V 2017 *Phys. Rev. E* **95** 032317
[32] Franović I, Omel'chenko O E and Wolfrum M 2018 *Chaos* **28** 071105
[33] Schülen L, Janzen D A, Medeiros E S and Zakharova A 2021 *Chaos Solitons Fractals* **145** 110670